Simulation of plunging breaking waves induced by a submerged bump

Qiu Jin, Dominic Hudson, Pandeli Temarel

Fluid Structure Interactions group, Faculty of Engineering and Physical Sciences,
University of Southampton
Southampton, UK

1. Introduction

Plunging wave breaking is one of the most violent phenomena in air-water interface interactions, producing strong turbulence with large amounts of air bubbles, sprays, jets and water droplets. Wave breaking phenomena are easily observed in ship bow and stern waves and they are one of the main sources of underwater noise and white-water wake. However, the process of plunging wave-breaking is not well understood and there are few studies that provide a detailed quantitative description of breaking waves. It is therefore important to investigate the conditions under which breaking appears and the interactions of air and water. This paper investigates a plunging breaking wave generated by a shallowly submerged bump positioned in a uniform flow.

Laboratory experiments provide a highly powerful investigative tool. Early experimental fluid dynamics (EFD) focus on qualitative descriptions of wave geometric properties[1], jet generation and air entrainment[2]. With the development of new measurement techniques, more recent EFD studies provide detailed velocity and turbulence data. A good example is represented by [3] in which a detailed and complete analysis of a plunging breaking wave is provided. However, even with recent sophisticated and highly resolved measuring techniques, it is not always possible to achieve a complete description of phenomena in highly aerated conditions [4].

In computational fluid dynamics (CFD) investigations, non-linear potential flow boundary integral methods or boundary element methods are widely used to predict the occurrence of breaking allowing studies of large computational domains [5]. Only the beginning of the non-linear wave deformation is captured in these models as they are unable to predict beyond the onset of wave breaking or merging. Recently, the Reynold's averaged Navier-Stokes equations have been solved to simulate the two-phase flow with surface capturing methods to describe the motion of the free-surface. Although having limitations, two-phase solvers allow a detailed investigation of the complex flow generated by the breaking of free surface waves. Wang et al. [6] identified three repeated plunging events with a Cartesian Grid, immersed boundary coupled Level Set and Volume of Fluid (CLSVOF) CFD method. Iafrati [4] numerically simulated the energy dissipation mechanisms in the breaking process of third-order Stokes waves with a Navier-Stokes solver combined with a Level Set method. Lubin [7] investigated the generation and evolution of aerated vortex filaments in plunging breaking waves.

This paper uses a two-phase flow solver in the open source RANS solver OpenFOAM to study the wave breaking process and the velocity fields generated by a shallowly submerged bump. The two-phase flow solver is first validated through comparison with experiments. The computational domain and boundaries are designed following the experiments conducted in [3]. The free surface evolution, wave breaking process and velocity fields are investigated around and downstream of the bump. The simulations are carried out using the standard RANS k-ω SST turbulence model with

an algebraic Volume of Fluid (AVOF) technique for the interface capturing.

2. Numerical methods

2.1. Governing equations

In the present work, a standard two-phase solver, interFoam, in the Open source platform OpenFOAM is used to simulate plunging breaking waves. Reynolds averaged Navier-Stokes equations are used to represent the motions of these two incompressible, isothermal and immiscible fluids. The governing equations, including mass and momentum conservation are expressed as:

$$\nabla \cdot \mathbf{U} = 0 \tag{1}$$

$$\frac{\partial \rho \mathbf{U}}{\partial t} + \nabla \cdot \left(\rho\left(\mathbf{U} - \mathbf{U_g}\right)\mathbf{U}\right) = -\nabla p_d - \mathbf{g} \cdot \mathbf{h} \nabla \rho + \nabla \cdot \left(\mu_{eff} \nabla \mathbf{U}\right) + (\nabla \mathbf{U}) \cdot \nabla \mu_{eff} + \mathbf{f}_\sigma \tag{2}$$

Where $\mathbf{U}$ is the fluid velocity and $\mathbf{U_g}$ is the grid velocity, ρ is the mixture density of the fluid, $p_d = p - \rho \mathbf{g} \cdot \mathbf{h}$ is the dynamic pressure which is obtained by subtracting the hydrostatic component from the total pressure, $\mathbf{g}$ is the gravity acceleration, $\mu_{eff} = \mu + \rho \nu_t$ is effective dynamic viscosity, μ is the dynamic viscosity and ν_t is the turbulence viscosity, f_σ is a surface tension term. For modeling turbulent flow, a standard k-ω Shear Stress Transport (SST) turbulence model is selected to solve the Reynold's stress, where k is the turbulent kinetic energy and ω is the turbulence specific dissipation rate:

$$k = 1.5(I|\mathbf{u}_{ref}|)^2, \tag{3}$$

$$\varepsilon = \frac{k^{0.5}}{C_\mu L}, \tag{4}$$

where *I* is the turbulence intensity, $\mathbf{u}_{ref}$ is the reference velocity, C_μ is a constant equal to 0.09, and L is a reference length scale.

In the present work, a Finite Volume Method (FVM) with structured grids is applied to discretize the computational domain. The PIMPLE (PISO-SIMPLE) algorithm is used for pressure velocity coupling, which is a hybrid of a Pressure Implicit Splitting Operator (PISO) algorithm and a Semi-Implicit Method for Pressure-Linked Equations (SIMPLE) algorithm.

2.2. Free surface

The interFoam solver uses an algebraic VOF (AVOF) to track the interface between air and water in a special algorithm called Multidimensional Universal Limiter for Explicit Solution (MULES). Using a phase indicator function α, the two immiscible fluids are considered as one effective fluid throughout the domain and no interface reconstruction process is applied during the calculation. The indicator α is the volume function, which is defined as the relative proportion of water in each cell. If $\alpha = 1$, the cell is full of water and if $\alpha = 0$, the cell is full of air, and in any other case the cell contains the interface between air and water. The transport equation for the phase indicator is shown as:

$$\frac{\partial \alpha}{\partial t} + \nabla \cdot (\mathbf{U}\alpha) = 0, \tag{5}$$

In MULES, an artificial compression term is added to the conventional transport equation, equation 6, to limit the amount of interface smearing:

$$\frac{\partial \alpha}{\partial t} + \nabla \cdot \left(\rho\left(\mathbf{U} - \mathbf{U_g}\right)\alpha\right) + \nabla \cdot (\mathbf{U_r}(1 - \alpha)\alpha) = 0, \tag{6}$$

where $\mathbf{U_r}$ is the artificial velocity field used to compress the interface and which takes effect only near the interface.

The surface tension plays an important role in plunging breaking waves since the pressure jump mainly depends on the curvature of the free surface. It is therefore necessary to take the surface tension into account to capture the free surface accurately. In the interFoam solver, the surface tension at the air-water interface generates an additional pressure gradient resulting in a force, which is evaluated per unit volume using the continuum surface tension (CSF) model:

$$\mathbf{f}_\sigma = \sigma\kappa\Delta\alpha, \tag{7}$$

where σ is surface tension, σ= 0.072 kg/s^2 in an air water system, κ is the mean curvature of the free surface and is defined as:

$$\kappa = -\nabla \cdot \frac{\nabla\alpha}{|\nabla\alpha|}. \tag{8}$$

3. Computational implementation

The geometry model is built from the bump profile with a height H=0.1143m in the experiment [3]. The origin of the coordinate system is placed at the centre of the bump. The simulations are conducted on a 2D computational domain of x/H= [-52, 44] and z/H= [0, 5]. The entire computational domain and the different boundaries applied at inlet, outlet, bottom, upper are shown in Fig. 1. The front and back boundary conditions are set as empty, since it is a two-dimensional simulation. The three-dimensional simulation with the same parameters as the experiment will be investigated in the future. The inlet velocity imposed at the inlet boundary is fixed with U=0.87 m/s for the water and 0 m/s for the air. The initial free surface elevation is set with a height of 2H, with a uniform velocity field of 0.87 m/s prescribed in the water domain, with the air phase at rest. The corresponding initial Re=$\rho uh/\mu$ = 107503 and Fr=$\rho/\sqrt{gh}$=0.789.

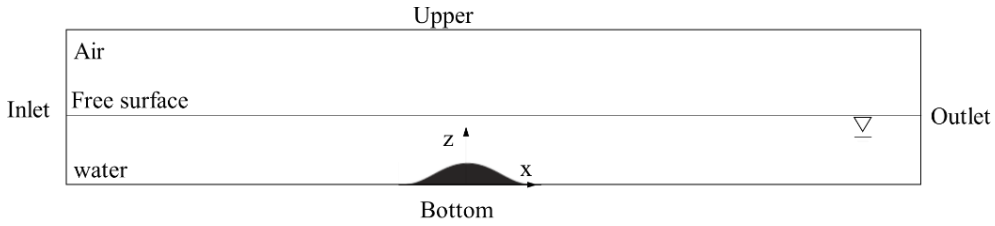

Fig. 1. Computational domain with boundaries.

The meshing of the blocks consists of conformal non-orthogonal structured elements throughout the whole computational domain. A more refined mesh is employed around the bump, the downstream area and free surface compared to the rest of the domain to capture better the near-wall turbulent flow and wave evolution.

Fig. 2. Mesh around the bump.

4. Results and discussion

4.1. Grid independency study

To check the grid independency of the results, three grids are applied in this study, with

consecutively increased (by a factor of 2) sizes from grid one with 154960 cells, to grid two with 348660 cells and grid three, 657984 cells. The maximum Courant number, Co, equals 0.5 in all these three cases. The wave profiles for the three grids are shown in Fig. 3. The overall structures of the interface obtained on the three grids are very similar. The jet tip is slightly sharper on the finest grid since a finer grid can capture more details of the free surface with higher grid resolution. In order to capture more detailed wave evolution and the velocity field, the finest mesh is chosen here for better understanding of the process of the plunging breaking waves.

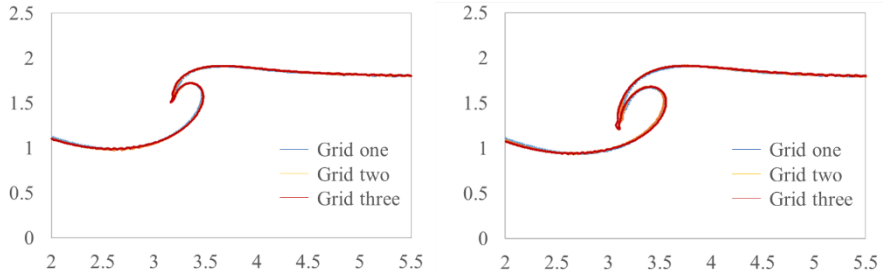

Fig. 3. Wave profiles with three different grids.

4.2. Wave breaking process

The plunging wave breaking process has been characterized in the previous studies (see [3]) by four major phases including steep wave formation, jet formation and overturning, splash-up and air entrainment. The major events of the plunging wave breaking are shown in Fig. 4 including instantaneous wave profiles from both experiments and CFD simulations. t_b is a reference time at which the wave reaches its maximum height [3], which is chosen as the initial time to compare the EFD and CFD results. The time instances do not match between the CFD and EFD due to differences in the initial conditions.

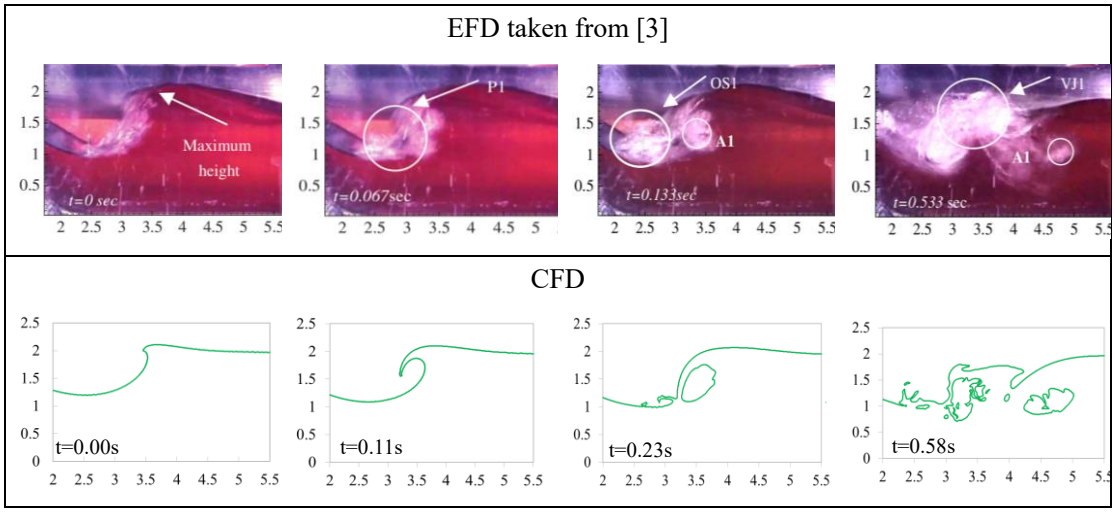

Fig. 4. Instantaneous free surface profiles of the wave breaking process.

At time t=0.0s, the wave crest becomes steepest when it reaches its maximum height and starts to overturn. The location and the wave profiles match quite well. At time t=0.11s, a jet of water is projected forward into a characteristic overturning motion. At time t=0.23s, the first plunge occurs when the overturning jet impinges onto the free surface of the tough. With the overturning jet, a large amount of air below the jet is entrapped which forms a big air bubble. Although the EFD and

CFD bubbles are located at almost the same place, the size of the air bubble is almost 2 times larger than the EFD results. Once the jet tip touches the trough surface, splash-up initiates and develops at the location where the jet impacts. As shown in both EFD and CFD plot, an oblique splash-up is generated towards the upstream direction with a spray region. The splash-up intensified and a vertical jet can be clearly observed in the CFD profiles and reaches its maximum height at t=0.58s. Severe bubble shape deformations can be seen at t=0.58s compared to t=0.23s in the CFD plot as the initially entrapped air bubble moves downstream. It is interesting to observed that the air bubble after the plunging collapsed in EFD but remains the same size in CFD. This may be because of 3D instability, which may contribute to the breaking of the air bubble. 3D simulations with same computational set-up will be investigated in the future.

4.3. Velocity field

Fig. 5 shows the EFD horizontal velocity, U, contours and the CFD U contours, respectively at the time steps that correspond to the wave breaking process in Fig. 4. For CFD results, air and water are presented separately, for clarification of the two-phase flow. All contour plots are presented in the same dimensional form.

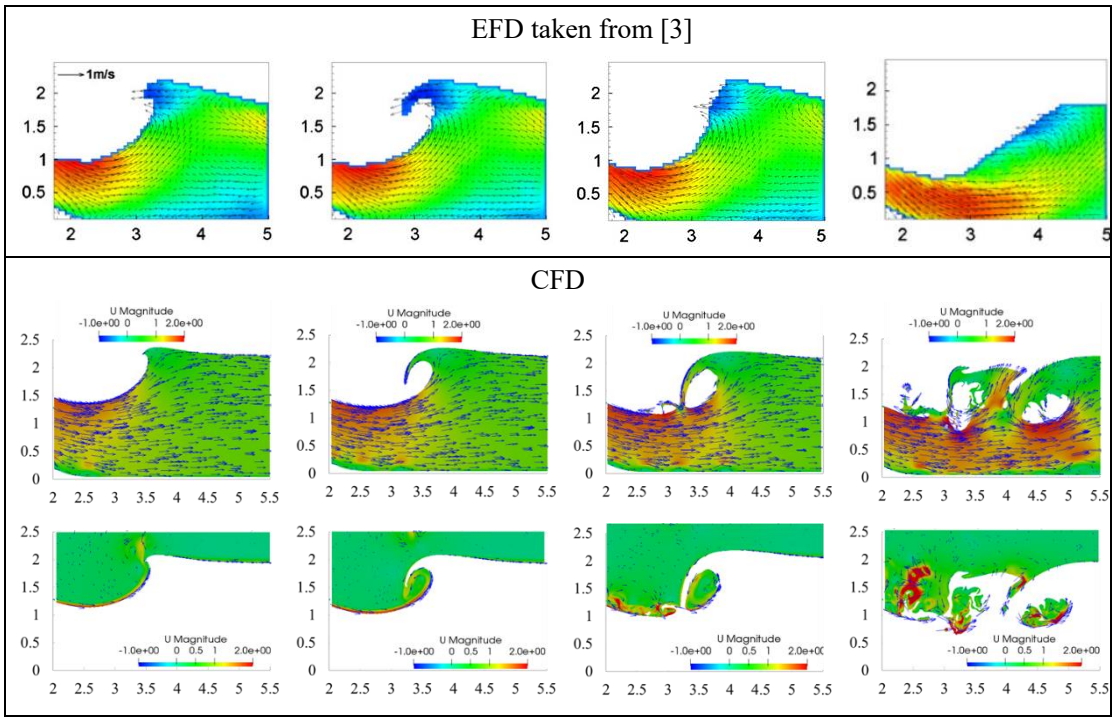

Fig. 5. Velocity fields of the wave breaking process.

The uniform inlet flow was accelerated by the bump and generated plunging breaking waves downstream of the bump. The velocity of the main region of air remains at zero but is increased close to the free surface. During the whole wave breaking process, the velocity in the back side is very high near the free-surface and then gradually decreased along the flow direction. At t=0s, a positive U region extends towards downstream of the bump and is reduced in the region where the steep wave crest is formed. At t=0.11s, a negative U region initiates in the wave crest and intensifies after the overturning jet. The region of bubbly flow increases after the wave crest plunges into the wave trough. The velocity data are not available in these regions through EFD. More detailed resolutions of splashing and vertical jet and bubble entrainment events in the wave breaking process

can be found in CFD simulations. At t=0.23s and t=0.58s, after the overturning jet hits the trough surface, strong air flows are induced with a series of vortices in both air and water.

5. Conclusion

A two-phase flow solver is applied for the simulation of the plunging breaking waves observed behind a shallowly submerged bump in a uniform flow. A standard k-ωSST turbulence model incorporated with the interface capturing algebraic Volume of Fluid (AVOF) method is adopted to captures the interface of air and water and the turbulent flow downstream of the bump.

Satisfactory agreement is observed between the numerical results and experimental data in the process of the plunging wave breaking. The major wave breaking events are revealed by CFD simulations and validated by EFD observations, including maximum wave height, first plunge, splash up and the air entrainment. The algebraic Volume of Fluid method with a k-ω SST turbulence model predicts successfully the formation of the plunging breaking wave and the measured velocity profiles.

For the plunging breaking wave, further investigation will focus on the detailed investigation of turbulent flow below the plunging breaking waves and its effect on the resulting waves. 3D simulation will be designed to investigate the instabilities in the third dimension which may contribute to the observed breaking of air bubbles.

The physics of the formation and break-up of the bubble or water jet is a complex multiphase flow problem. Since the interface is modelled by the AVOF capturing method, the air bubbles or water droplets are unable to be captured when the scale is smaller than the grid spacing. A finer mesh will be designed to get a better understanding of the plunging breaking waves. Besides of the gridding problems, unphysical tearing of the free surface tends to occur due to a large density jumps between the air and the water across the free surface. A physical-based smoothing procedure is required to resemble the viscous boundary layer near the free-surface.

6. References

[1] P. Bonmarin, “Geometric properties of deep-water breaking waves,” *J. Fluid Mesh*., vol. 209, no. 1952, 1989.

[2] H. Chanson and L. Jaw-Fang, “Plunging jet characteristics of plunging breakers,” *Coast. Eng*., vol. 31, no. 1–4, pp. 125–141, 1997.

[3] D. Kang, S. Ghosh, G. Reins, B. Koo, Z. Wang, and F. Stern, “Impulsive plunging wave breaking downstream of a bump in a shallow water flume-Part I: Experimental observations,” *J. Fluids Struct.*, vol. 32, pp. 104–120, 2012.

[4] A. Iafrati, “Energy dissipation mechanisms in wave breaking processes: Spilling and highly aerated plunging breaking events,” *J. Geophys. Res*., vol. 116, pp. 1–22, 2011.

[5] A. Babanin, D. Chalikov, I. Young and I. Savelyev, “Numerical and laboratory investigation of breaking of steep two-dimensional waves in deep water,” *J. Fluid Mesh.*, vol. 644, pp. 433–463, 2010.

[6] Z. Wang, J. Yang, B. Koo, and F. Stern, “A coupled level set and volume-of-fluid method for sharp interface simulation of plunging breaking waves,” *Int. J. Multiph. Flow*, vol. 35, no. 3, pp. 227–246, 2009.

[7] P. Lubin and S. Glockner, “Numerical simulations of three-dimensional plunging breaking waves : generation and evolution of aerated vortex filaments,” *J. Fluid Mesh*., vol. 767, pp. 364–393, 2015.